

Current characteristics of strands weaved by transposed REBCO tapes

Heng Zhang(张恒), Jing-Yi Yang(杨敬伊), Zong-Li Wei(魏宗礼), and Wei Pi(皮伟)
Citation: Chin. Phys. B, 2026, 35 (**7**): 077402. DOI: 10.1088/1674-1056/ae181f
http://cpb.iphy.ac.cn; http://iopscience.iop.org/cpb

What follows is a list of articles you may be interested in

Cu1234 single crystals growth with contamination-free quality

Haoyu Zheng(郑皓宇), Luchuan Shi(史鲁川), Xiaoming Chen(陈晓铭), Yuling Dai(戴玉玲), Kai Huang(黄凯), Yi Peng(彭毅), Jianfa Zhao(赵建发), Xiancheng Wang(望贤成), and Changqing Jin(靳常青)
Chin. Phys. B, 2026, 35 (**5**): 057406. DOI: 10.1088/1674-1056/ae4d28

Large grain size obtained by substrate directly heating for YBCO epitaxial films

Kebin Li(李珂彬), Yifei Zhang(张一飞), Tong Zhang(张同), Shuguang Yi(易曙光), Shi-Peng Zhang(张世鹏), Quan-Ming Gao(高全明), and Shan-Dong Li(李山东)
Chin. Phys. B, 2025, 34 (**9**): 097403. DOI: 10.1088/1674-1056/add4fc

Fabrication and characterization of MgB_2 spherical shells with reduced thickness on 1 mm diameter Si_3N_4 spheres

Ruining Sun(孙瑞宁), Tiequan Xu(徐铁权), Yue Wang(王越), Furen Wang(王福仁), and Zizhao Gan(甘子钊)
Chin. Phys. B, 2025, 34 (**7**): 077402. DOI: 10.1088/1674-1056/adcdec

Role of grain boundary networks in vortex motion in superconducting films

Yu Liu(刘宇), Feng Xue(薛峰), and Xiao-Fan Gou(苟晓凡)
Chin. Phys. B, 2023, 32 (**12**): 127401. DOI: 10.1088/1674-1056/ace315

Flux pinning evolution in multilayer Pb/Ge/Pb/Ge/Pb superconducting systems

Li-Xin Gao(高礼鑫), Xiao-Ke Zhang(张晓珂), An-Lei Zhang(张安蕾), Qi-Ling Xiao(肖祁陵), Fei Chen(陈飞), and Jun-Yi Ge(葛军饴)
Chin. Phys. B, 2023, 32 (**3**): 037402. DOI: 10.1088/1674-1056/ac89e1

Current characteristics of strands weaved by transposed REBCO tapes

Heng Zhang(张恒)[1], Jing-Yi Yang(杨敬伊)[2], Zong-Li Wei(魏宗礼)[3], and Wei Pi(皮伟)[1,†]

[1] *State Key Laboratory of Alternate Electrical Power System with Renewable Energy Sources and the Key Laboratory of HV and EMC Beijing, North China Electric Power University, Beijing* 102206, *China*

[2] *State Grid Tangshan Power Supply Company, Tangshan* 063100, *China*

[3] *State Grid Haibei Power Supply Company, Haiyan* 812299, *China*

(Received 13 September 2025; revised manuscript received 6 October 2025; accepted manuscript online 28 October 2025)

A superconducting strand, fabricated by weaving 3, 5, 7, or more transposed rare-earth barium copper oxide (REBCO) high-temperature superconducting (HTS) tapes, is proposed to enhance the critical current and achieve uniform distributions of operating current in each REBCO tape. This design allows all the HTS tapes to quench simultaneously, thereby increasing the critical current compared to a strand simply stacked with HTS tapes and improving HTS tape utilization. Additionally, the transposition strategy can be used to manufacture strands woven with more REBCO tapes for high-current applications such as power transmission. Experimental results demonstrate that strands woven with HTS tapes can enhance the critical current in comparison with strands simply stacked and Roebel cables. Furthermore, a finite element model (FEM) based on the H-formulation has been established to show the operating current distribution.

Keywords: multiple transposed HTS tapes, H-formulation, critical current, HTS tape utilization (β_i), normalized operating current

PACS: 74.70.–b

DOI: 10.1088/1674-1056/ae181f **CSTR:** 32038.14.CPB.ae181f

1. Introduction

Previous studies have extensively investigated the relationships between economic growth, environmental degradation, and energy consumption. It is well established that significant energy is required to sustain these developments.[1,2] Nuclear fusion is a promising approach for developing sustainable energy sources. However, the fundamental challenge is to generate a high magnetic field capable of shaping and sustaining high-temperature plasma inside the tokamak vessel.[3] Traditional electric power transmission and other applications can result in significant energy losses.[4]

Therefore, the adoption of superconducting technology is essential to satisfy the demands of generating high magnetic fields while minimizing energy losses. Second-generation (2G) high-temperature superconducting (HTS) materials, such as rare-earth barium copper oxide (REBCO) tapes, exhibit improved mechanical properties and higher current-carrying capacities than those of conventional conductors.[5–11]

Several approaches have been developed to fabricate HTS strands, including twisted stacked strands,[12] conductors on round core (CORC) strands,[12–14] round twisted stacked conductors,[15–17] HTS strand-in-conduit conductors (CICC),[18,19] X-cables,[20,21] and Roebel strands.[22] In particular, the Roebel strand design enables the full transposition of HTS tapes, thereby facilitating current distribution across the tapes, which in turn enhances the overall performance. This includes an evenly distributed operating current, a reduction in the magnetic flux density, and an improvement in the efficiency of the tapes. Previous research has considered the number of HTS tapes, transposition length, twist pattern, tape width, bending radius, and thickness of the Roebel strand.[23–29] In a typical Roebel design, HTS tapes are cut into trapezoidal shapes and assembled into strands. This process results in notable wastage of HTS material. In addition, a similar structure to the Roebel cable, the X-cable, requires in-plane bending to achieve transposition. The punching process of Roebel cables or local in-plane bending in X-cables may induce microstructural modifications in the HTS tapes, potentially leading to local critical current degradation.[21,30]

This paper presents a method for making HTS strands that employs a weaving technique. Unlike conventional approaches, this method eliminates cutting HTS tapes and minimizes in-plane and out-of-plane bending deformation. Meanwhile, the HTS tapes undergo complete transposition, exhibiting spatial transposition symmetry that ensures a uniform current distribution across each tape. Consequently, it is expected that all the tapes will reach the critical state simultaneously. An optimized tape arrangement reduces magnetic flux density and increases critical current compared to simply stacked strands. Experimental results demonstrate that woven HTS strands exhibit superior current-carrying capacity relative to both simply stacked strands and Roebel cables. Furthermore,

†Corresponding author. E-mail: ppiiwei@ncepu.edu.cn

© 2026 Chinese Physical Society and IOP Publishing Ltd. All rights, including for text and data mining, AI training, and similar technologies, are reserved.

this technique can be extended to manufacture strands woven with more REBCO tapes for high-current applications, particularly in power transmission systems.

2. Structure and parameters

Figures 1–3 illustrate the process of manufacturing the HTS strands woven using 3, 5, and 7 REBCO tapes. The transposition strategy can be used to manufacture strands woven with N ($N \geq 3$) REBCO tapes.

As shown in Fig. 1, the transposition strategy employed in the HTS strand is as follows: the sequence $(1,2,3) \rightarrow (1,3,2) \rightarrow (3,1,2) \rightarrow (3,2,1) \rightarrow (2,3,1) \rightarrow (2,1,3) \rightarrow (1,2,3) \rightarrow \cdots$ is defined as the transposition cycle in a strand woven with 3 REBCO tapes. The distance along the strand between step 1 and step 9 can be defined as the transposition length.

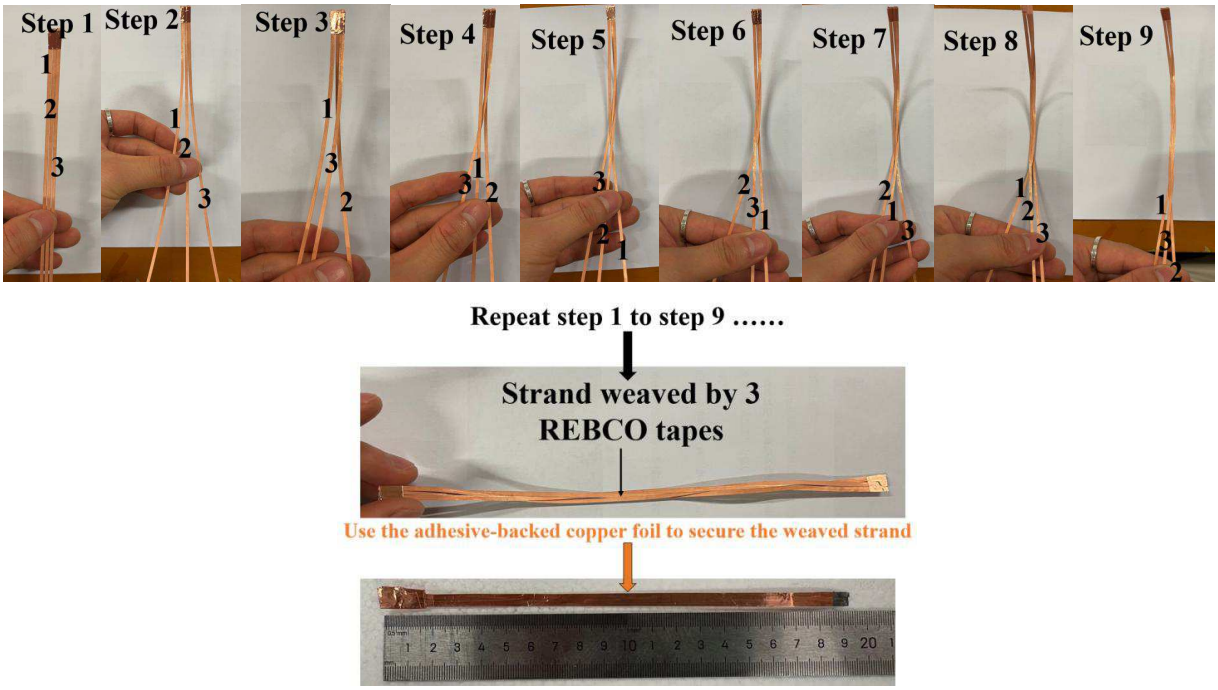


Fig. 1. Manufacturing process of the HTS strand woven with 3 REBCO tapes.

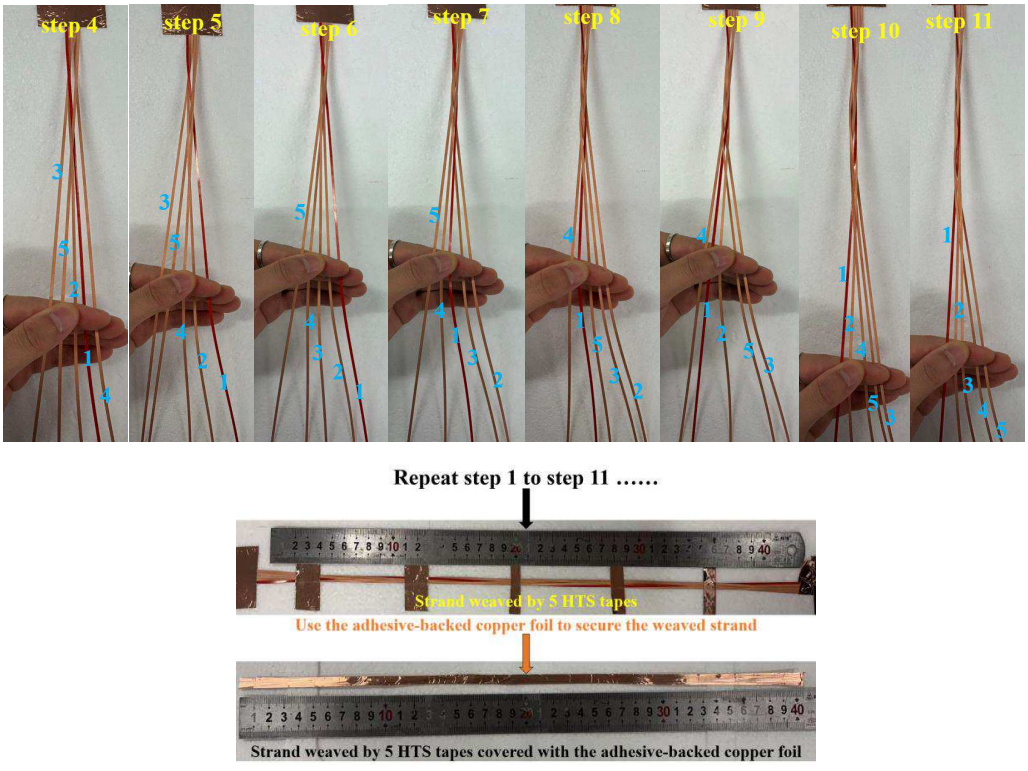


Fig. 2. Manufacturing process of the HTS strand woven with 5 REBCO tapes.

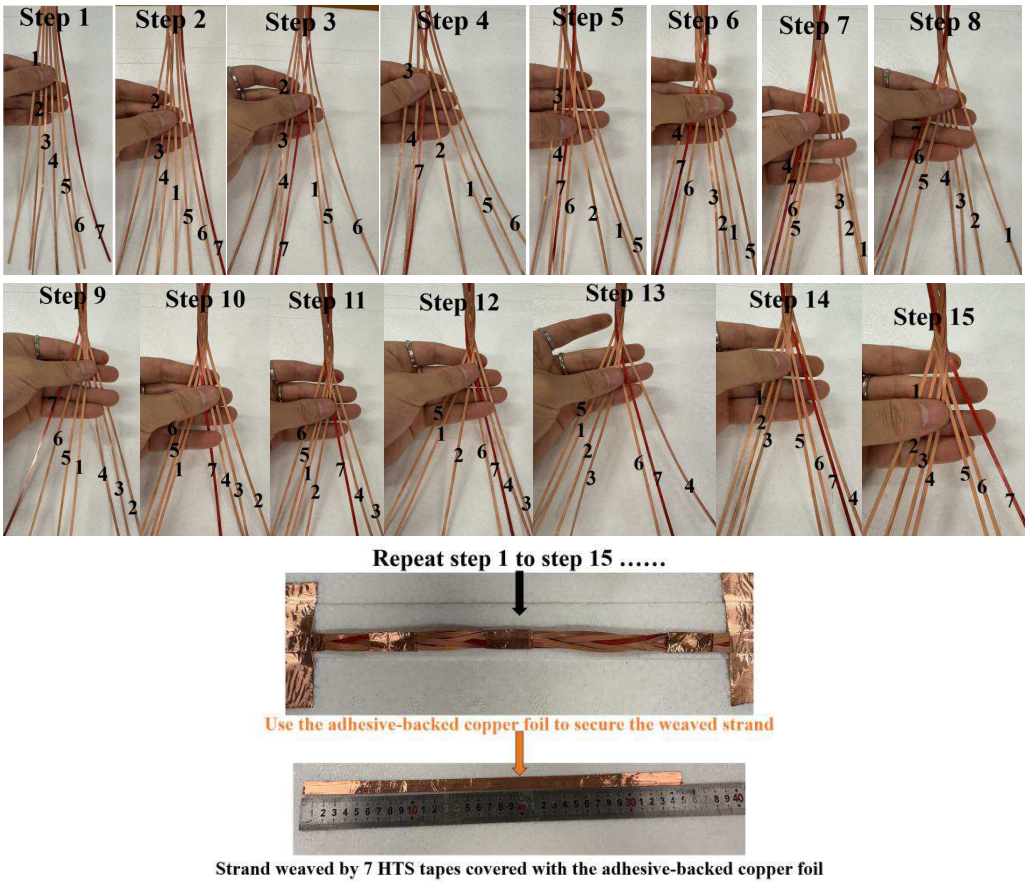


Fig. 3. Manufacturing process of the HTS strand woven with 7 REBCO tapes.

As shown in Fig. 2, the transposition strategy employed in the HTS strand is as follows: the sequence of transformations is $(1,2,3,4,5) \rightarrow (1,2,5,3,4) \rightarrow (2,5,1,3,4) \rightarrow (2,5,4,1,3) \rightarrow (5,4,2,1,3) \rightarrow (5,4,3,2,1) \rightarrow (4,3,5,2,1) \rightarrow (4,3,1,5,2) \rightarrow (3,1,4,5,2) \rightarrow (3,1,2,4,5) \rightarrow (1,2,3,4,5) \cdots$. This sequence defines the transposition cycle for a strand woven with 5 REBCO tapes. The distance along the strand between step 1 and step 11 can be defined as the transposition length. By adjusting the transposition length, both in-plane and out-of-plane bending of the tapes can be minimized or prevented.

As shown in Fig. 3, the transposition strategy employed in the HTS strand is as follows: the sequence of numbers is $(1,2,3,4,5,6,7) \rightarrow (2,3,4,1,5,6,7) \rightarrow (2,3,4,7,1,5,6) \rightarrow (3,4,7,2,1,5,6) \rightarrow (3,4,7,6,2,1,5) \rightarrow (4,7,6,3,2,1,5) \rightarrow (4,7,6,5,3,2,1) \rightarrow (7,6,5,4,3,2,1) \rightarrow (7,6,5,1,4,3,2) \rightarrow (6,5,1,7,4,3,2) \rightarrow (6,5,1,2,7,4,3) \rightarrow (5,1,2,6,7,4,3) \rightarrow (5,1,2,3,6,7,4) \rightarrow (1,2,3,5,6,7,4) \rightarrow (1,2,3,4,5,6,7) \rightarrow \cdots$. This sequence defines the transposition cycle for a strand woven with 7 REBCO tapes. The distance along the strand between step 1 and step 15 can be defined as the transposition length of the strand woven with seven REBCO tapes. It is evident that adjustment of the transposition length enables the minimization or elimination of both in-plane and out-of-plane tape bending.

Table 1. Main parameters of the REBCO tape.

Geometrical parameters	Items	Values
Width	REBCO tape	2 mm
Thickness	Silver layer	3 μm
Thickness	Copper layer	18 μm
Thickness	Substrate layer	50 μm
Thickness	REBCO tape	90 μm
Thickness	REBCO layer	1 μm
Mass density	REBCO	6.38 g/cm^3@300 K
Young's modulus (E)	REBCO	97 MPa@77 K
Poisson's ratio (ν)	REBCO	0.3
Critical current	Single REBCO tape	80 A@77 K

Table 1 lists the geometrical parameters of the REBCO tape provided by Shanghai Superconductor Technology Co., Ltd. The measured critical current of a single tape is 80 A, and the n index is 20.

3. FEM model and experimental schematic

3.1. FEM model

In this study, the H-formulation is used to develop a finite element model (FEM) for the simulation.

The governing equation (5) is as follows:[31]

$$\nabla \times (\rho(J_{\text{norm}}) \nabla \times \boldsymbol{H}) = -\frac{\mu_0 \mu_{\text{r}} \partial \boldsymbol{H}}{\partial t}. \tag{1}$$

In the simulation, the relative permeability (μ_{r}) is set to 1.

The vacuum permeability (μ_0) is a fundamental constant of $4\pi \times 10^{-7}$ (N/A^2).

The electrical characteristics of a superconducting material can be described by the E–J curve, and the equivalent electrical resistivity can be expressed as follows, given that $E_0 = 1$ μV/cm and $n = 20$

$$\rho(J_{\text{norm}}) = \frac{E_0}{J_c(\boldsymbol{B})} \cdot \left(\frac{J_{\text{norm}}}{J_c(\boldsymbol{B})} \right)^{n-1}, \tag{2}$$

$$J_c(\boldsymbol{B}) = J_{c0} \left(1 + \frac{1}{B_0} \sqrt{k^2 B_{\parallel}^2 + B_{\perp}^2} \right)^{-\alpha}, \tag{3}$$

where $k = 0.25$, $\alpha = 0.6$, and $B_0 = 0.02$ T.[32]

The boundary condition in the cross section of the HTS tape in the FEM model is calculated using the following formula:

$$I = \iint \boldsymbol{J} \cdot \mathrm{d}\boldsymbol{S}, \tag{4}$$

where α_i is the normalized operating current, and i takes a value from 1 to n, where n denotes the number of HTS tapes in the strand. For each tape, I_i represents the current in use, whereas I_{tot} is the operating current in the strand.

$$\alpha_i = \frac{I_i}{I_{\text{tot}}}, \tag{5}$$

where β_i is used to evaluate the utilization of the HTS tapes. I_{c0} is the critical current for individual HTS tapes in the absence of an external magnetic field.

$$\beta_i = \frac{I_{\text{tot}}}{n I_{c0}}. \tag{6}$$

3.2. Experimental schematic

The E–J characteristics of the HTS strands were measured using a conventional four-probe testing method, with a criterion of 1 μV/cm.

Figure 4 shows a schematic diagram of the experimental setup.

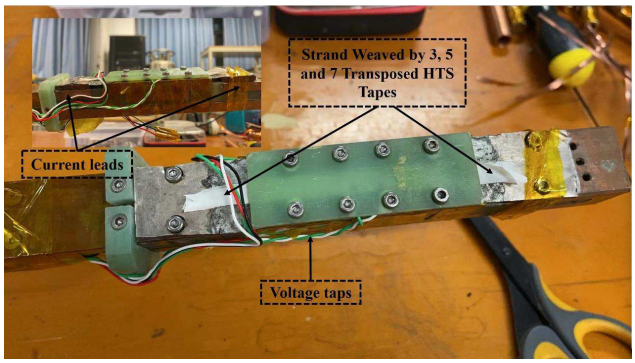


Fig. 4. Schematic diagram of the experimental measurement setup.

4. Result and discussion

4.1. Results of the strand stacked with 3, 5, and 7 HTS tapes

As shown in Fig. 5, the experimental E–I curves for strands stacked with 3, 5, and 7 HTS tapes exhibit critical currents of 156 A, 271 A, and 364 A, respectively. These values align closely with the simulated results (152 A, 275 A, and 371 A).

Figure 6 shows the magnetic flux density distribution in a strand stacked with 5 HTS tapes. The black arrows indicate the direction of the magnetic flux. Within the strand, the antiparallel B-field components cancel each other out, reducing the net magnetic flux density and current. The magnetic flux is primarily concentrated at the edges of the strand, indicating that the operating current flows mainly along the periphery. This indicates that the HTS tapes in the central region are underutilized, as illustrated in Fig. 7.

The operating current is primarily distributed in Tapes 1 and 5, with a comparatively lower current distribution in Tapes 2, 3, and 4, as shown in Fig. 7. Notably, Tape 3 exhibits the lowest utilization rate. As the operating current in Tapes 1 and 5 approaches their critical currents, the entire strand composed of 5 stacked HTS tapes will quench. However, Tapes 2, 3, and 4 remain below their critical currents. This uneven current distribution explains why the critical current of the strand woven with 5 HTS tapes is higher than that of the strand composed of 5 stacked HTS tapes.

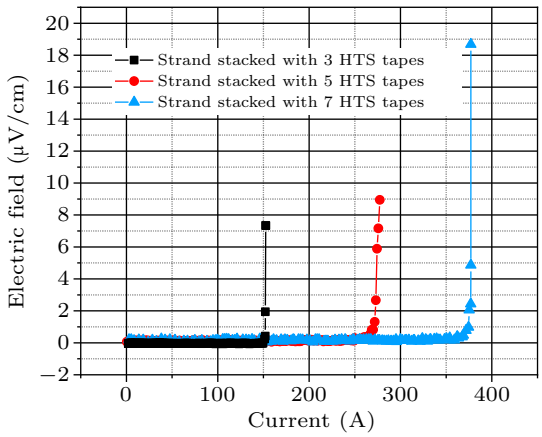


Fig. 5. The electric field intensity as a function of current in the HTS strands stacked with 3, 5, and 7 HTS tapes measured by experiments.

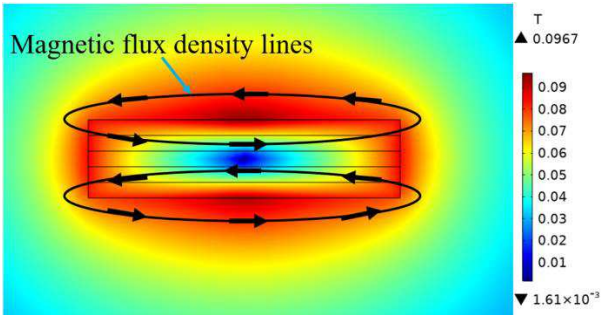


Fig. 6. Magnetic flux density distribution in the strand stacked with 5 HTS tapes at an operating current of 275 A.

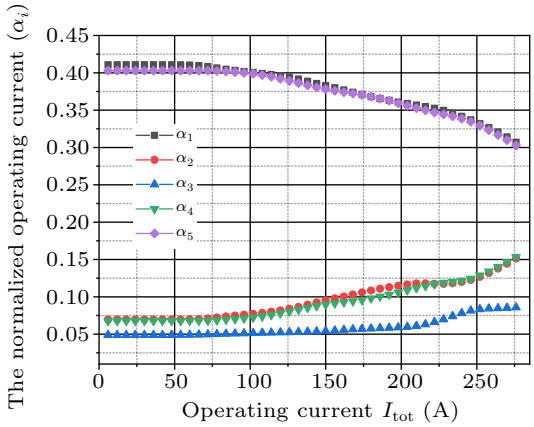


Fig. 7. Normalized operating current in the strand stacked with 5 HTS tapes.

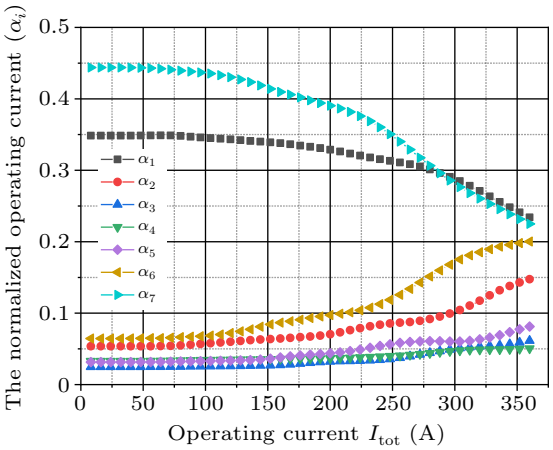


Fig. 8. Distribution of the normalized operating current in the strand stacked with 7 HTS tapes.

As shown in Fig. 8, the operating current is primarily distributed in Tapes 1 and 7, with a comparatively lower current distribution in Tapes 2 and 6. Notably, Tapes 3, 4, and 5 exhibited the lowest utilization rate. Furthermore, as the operating current in Tapes 1 and 7 approaches the critical current, the entire strand composed of 7 stacked HTS tapes will quench. However, Tapes 2, 3, 4, 5, and 6 remain below their critical currents. As a result of this uneven current distribution, a strand woven with 7 HTS tapes exhibits a higher critical current than a strand composed of 7 stacked HTS tapes.

4.2. Results of the strand woven with 3, 5, and 7 transposed HTS tapes

Figure 9 shows the measured *E–I* curves of HTS strands woven with 3, 5, and 7 transposed HTS tapes, and the critical currents are 190 A, 324 A, and 441 A, respectively. The simulated values are 181 A, 323 A, and 431 A, respectively.

Figure 10 illustrates the magnetic flux density distribution in the strand woven with 5 transposed HTS tapes obtained by simulation. Owing to the full and periodic transposition of the HTS tapes, each tape in the strand plays an equal role in carrying the operating current. As a result, the operating current is uniformly distributed across all tapes, allowing for the most

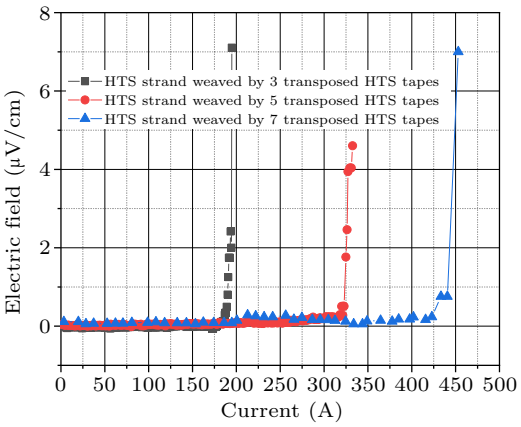


Fig. 9. The *E–I* curves of the HTS strands woven with 3, 5, and 7 transposed HTS tapes measured experimentally.

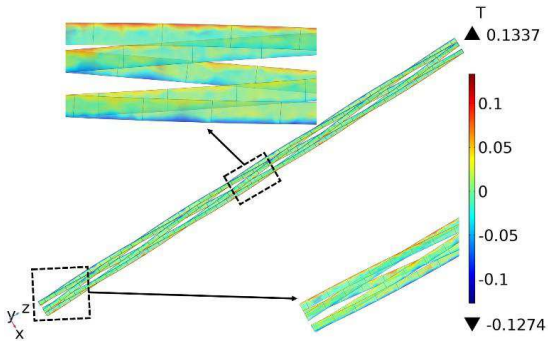


Fig. 10. Magnetic flux density in the strand woven with 5 transposed HTS tapes at an operating current of 323 A.

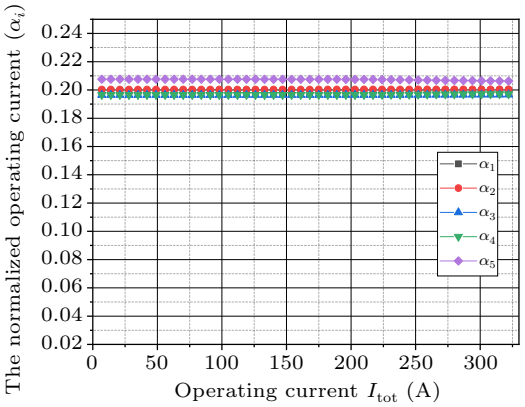


Fig. 11. Distribution of the normalized operating current in the strand woven with 5 transposed HTS tapes.

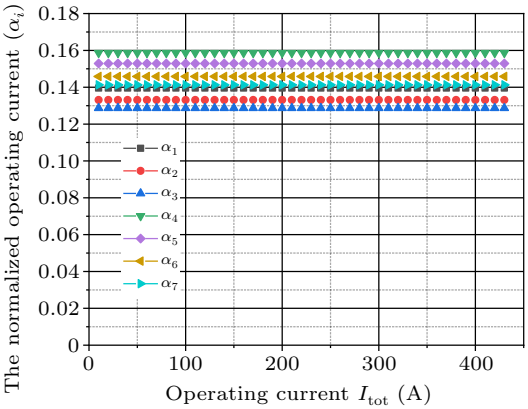


Fig. 12. Normalized operating current in the seven tapes of the strand woven with 7 transposed HTS tapes.

Figures 11 and 12 show the distribution of the normalized operating current in strands woven with 5 and 7 transposed HTS tapes, respectively. The operating current is distributed uniformly across all tapes owing to the fully periodic geometric structure of the strands. This uniform distribution means that all tapes in both the 5- and 7-tape strands will reach the critical state simultaneously, thus improving HTS tape utilization.

4.3. Comparison between strands woven and stacked with 3, 5, and 7 HTS tapes

Table 2 shows the experimental and simulated critical currents, magnetic flux density, and utilization factor (β_i) of the HTS tapes for the studied strands. The HTS strands woven with transposed HTS tapes improve HTS tape utilization, thereby increasing the critical current compared to strands simply stacked with HTS tapes.

Table 2. Comparison between the strands stacked and weaved by HTS tapes.

Items \ Strands	Stacked with 3 HTS tapes	Stacked with 5 HTS tapes	Stacked with 7 HTS tapes	Weaved by 3 HTS tapes	Weaved by 5 HTS tapes	Weaved by 7 HTS tapes	Roebel cable
The measured I_c	156	271	364	190	324	441	–
The simulated I_c	152	275	371	181	323	431	
Magnetic flux density (T)	0.086	0.097	0.123	0.084	0.134	0.140	
The measured β_i	65.0%	67.8%	65.0%	79.2%	81.0%	78.8%	53.0%–69.0%[24,30]
The simulated β_i	63.3%	68.8%	66.3%	75.4%	80.8%	77.0%	–

5. Conclusion

Based on the results and discussion, it can be concluded that due to the full transposition of HTS tapes, the operating current is uniformly distributed in each HTS tape, leading to a balanced magnetic flux density and improved tape utilization factor (β_i) and critical current. These results demonstrate that the woven strands exhibit superior performance in high-current applications such as power transmission.

Acknowledgments

Project supported by the National Natural Science Foundation of China (Grant No. 52277025) and the Beijing Natural Science Foundation (Grant No. 3252022).

References

[1] Xing H W, Husain S, Simionescu M, Ghosh S and Zhao X 2024 *Gondwana Res.* **129** 220
[2] Nuţă F M, Sharafat A, Abban O J, Khan I, Irfan M, Nuţă A C, Dankyi A B and Asghar M 2024 *Gondwana Res.* **128** 52
[3] Kerboua-Benlarbi S, Nouailletas R, Faugeras B, Nardon E and Moreau P 2024 *IEEE Trans. Plasma Sci.* **52** 2075
[4] Kim S K, Dinh M C, Choi J, Park M, Yu I K, Lee S and Sim K 2015 *IEEE Trans. Appl. Supercond.* **25** 4600205
[5] Larbalestier D C, Gurevich A, Feldmann D M and Polyanskii A 2001 *Nature* **414** 368
[6] Yu A B, Lin C T, Zhang X F and You L X 2023 *Chin. Phys. B* **32** 067402
[7] Xiong P Y, Chen F C, Feng Z P, Yang J T, Xia Y D, Yuan Y F, Wang X, Yuan J, Wu Y, Shi J and Jin K 2023 *Chin. Phys. B* **32** 077402
[8] Fetisov S S, Zubko V V, Zanegin S Y, Nosov A A, Vysotsky V S, Kario A, Kling A, Goldacker W, Molodyk A, Mankevich A, Kalitka V, Adamenkov A, Samoilenkov S and Melyukov D 2016 *IEEE Trans. Appl. Supercond.* **26** 4803204
[9] Dong H, Huang D X, Yu H, Gu H W and Ding F Z 2025 *Chin. Phys. B* **34** 070702
[10] Sytnikov V and Lelekhov S 2021 *IEEE Trans. Appl. Supercond.* **31** 4201405
[11] Zhang Y F, Chen Y, Li X, Wang Z, Liu J and Zhao H 2024 *Chin. Phys. Lett.* **41** 117402
[12] Choi K, Han J, Lee J K and Kim W S 2023 *IEEE Trans. Appl. Supercond.* **33** 5901005
[13] Mulder T, Dudarev A, Mentink M, van der Laan D, Dhallé M and ten Kate H 2016 *IEEE Trans. Appl. Supercond.* **26** 4803705
[14] Zhu Z, Wang Y, Xing D, Pei X, Zhang M and Yuan W 2019 *IEEE Trans. Appl. Supercond.* **29** 4801905
[15] Uglietti D, Bykovsky N, Wesche R and Bruzzone P 2015 *IEEE Trans. Appl. Supercond.* **25** 4202106
[16] Bykovsky N, Uglietti D, Wesche R and Bruzzone P 2015 *IEEE Trans. Appl. Supercond.* **25** 4800304
[17] Uglietti D, Wesche R and Bruzzone P 2014 *IEEE Trans. Appl. Supercond.* **24** 4800704
[18] Mulder T, Dudarev A, Mentink M, Dhallé M and ten Kate H 2016 *IEEE Trans. Appl. Supercond.* **26** 4801704
[19] Zhu Y H 2002 *Proc. 19th IEEE/NPSS Symp. Fusion Eng.* (Atlantic City, NJ) p. 380
[20] Wang J, Kang R, Chen X, Yang C, Wang Y Z, Wang C T and Xu Q G 2022 *Supercond.* **3** 100019
[21] Wang J, Kang R, Wang Y Q, Chen X, Wang C T, Wang Y Z, Yang H, Li C Y, Ning F P, Zhao L, Hou Z L, Ma T, Dai S T and Xu Q J 2024 *IEEE Trans. Appl. Supercond.* **34** 4802105
[22] Fleiter J, Ballarino A, Bottura L, Goldacker W and Kario A 2015 *IEEE Trans. Appl. Supercond.* **25** 4802404
[23] Bélec M, Guddemi C and Millet C 2012 *Proc. IEEE Int. Conf. Cond. Monit. Diagn. (Bali)* pp. 412
[24] Lombardo V, Barzi E, Turrioni D, Zlobin A V, Long N J and Badcock R A 2011 *IEEE Trans. Appl. Supercond.* **21** 2331
[25] Pelegrin J, Bailey W and Yang Y 2021 *IEEE Trans. Appl. Supercond.* **31** 4802305
[26] Higashikawa K, Guo X, Inoue M, Jiang Z N, Badcock R, Long N and Kiss T 2017 *IEEE Trans. Appl. Supercond.* **27** 8001404
[27] Grilli F and Zermeño V M R 2017 *IEEE Trans. Appl. Supercond.* **27** 6603605
[28] Bumby C W, Badcock R A and Long N J 2013 *IEEE Trans. Appl. Supercond.* **23** 4801805
[29] Gijoy S and Roy K E R 2021 *IEEE Trans. Appl. Supercond.* **31** 6600107
[30] Grilli F, Vojenčiak M, Kario A and Zermeño V 2016 *IEEE Trans. Appl. Supercond.* **26** 4803005
[31] Shen B, Grilli F and Coombs T 2020 *IEEE Access* **8** 1
[32] Wang Y S 2013 *Fundamental Elements of Applied Superconductivity in Electrical Engineering* (Singapore: John Wiley & Sons) pp. 52